Malaysian Journal of Chemistry, 2025, Vol. 27(4), 126-143

Removal of Urea by Adsorption using Solid Sorbent from Photovoltaic Industry Waste

Nur Hidayah Deeleanie[1], Nur Imanina Farhana Japar[1], Azizul Hakim Lahuri[1]*, Syawal Mohd Yusof[1], Siti Sarahah Sulhadi[1], Ainil Hafiza Abdul Aziz[1], Salma Samidin[2], Mohd Azlan Kassim[3] and Wan Nor Roslam Wan Isahak[4]

[1]Department of Science and Technology, Universiti Putra Malaysia Sarawak, Nyabau Road, P. O. Box 396, 97008 Bintulu, Sarawak, Malaysia

[2]Department of Chemical and Process Engineering, Faculty of Engineering and Built Environment, Universiti Kebangsaan Malaysia, 43600 UKM Bangi, Selangor, Malaysia

[3]Green Solvent and Processes Team, Research Centre for Carbon Dioxide Capture and Utilisation (CCDCU), School of Engineering and Technology, Sunway University, No. 5 Jalan Universiti, Bandar Sunway, Petaling Jaya 47500, Selangor, Malaysia

[4]Department of Chemical and Process Engineering, Faculty of Engineering and Built Environment, Universiti Kebangsaan Malaysia, 43600 UKM Bangi, Selangor, Malaysia

*Corresponding author (azizulhakim@upm.edu.my)

This study focuses on addressing environmental concerns arising from the growth of the agricultural sector especially in relation to the inadequate treatment of wastewater from agricultural effluent. Urea is a prevalent component in agricultural wastewater due to its widespread use as a fertilizer, and contributes significantly to nutrient runoff, which can lead to eutrophication, biodiversity loss, and disruption of aquatic ecosystems. This research aligns with the United Nations Sustainable Development Goals (SDG) 2030, particularly Goal 6 (Clean Water and Sanitation) and Goal 12 (Responsible Consumption and Production), by proposing innovative solutions for wastewater management and industrial waste reutilization. This work introduces the novel approach of using a solid adsorbent derived from photovoltaic waste for the effective removal of urea from aqueous solution. By utilizing waste material, this approach not only promotes sustainability, but highlights the dual benefits of mitigating industrial waste and addressing agricultural wastewater challenges. The alkaline sludge (AS) used in this study was obtained from the photovoltaic industry in Sarawak, Malaysia. The findings indicate that the most efficient adsorbent for urea removal was calcined alkaline sludge (CAS). Its effectiveness was attributed to the presence of SiO_2 and $CaSiO_3$, which likely provided active adsorption sites, despite a lower BET surface area primarily contributed by micropores and mesopores. Optimal urea adsorption conditions were achieved at an initial urea concentration of 30 mg/L, with an adsorbent loading of 0.2 g, a temperature of 40 °C, and an adsorption period of 6 hours. Under these conditions, the removal percentage of CAS was 82.50 %, with an adsorption capacity of 4.95 mg/g. A slightly elevated temperature of 40 °C enhanced adsorption by increasing the kinetic energy of the molecules within the system. The adsorbed urea was measured through a weight loss of 10.85 % in the temperature range of 450–720 °C. This study not only demonstrates a sustainable approach to managing agricultural wastewater, but also underscores the potential of repurposing photovoltaic industry waste into effective adsorbents. Future research could explore scaling up this approach and investigating its application to other contaminants in agricultural and industrial wastewater.

Keywords: Alkaline sludge (AS); adsorption; photovoltaic industry waste; urea; adsorbent

Received: November 2024; Accepted: March 2025

The global population of 8 billion people [1] and the increasing demand for food resources have led to an expansion of the agricultural sector. The agricultural sector is also the backbone of a country's development, providing employment for locals, ensuring food security, and helping to foster favourable trade relations. However, this has driven massive land conversions from the natural ecosystem in order to supply sufficient resources for the population [2], and is responsible for the high levels of environmental pollutants. The aim of agricultural industrialization was to increase productivity in livestock, poultry, fish, and crop production, while relying on chemical fertilizers and mechanization. Utilization of chemical fertilizers refers to synthetic compounds containing nitrogen (N), phosphorus (P), potassium (K) or other elements. These are cheaper than organic fertilizers and have varying nutrient contents suitable for different

needs, making them more accessible to farmers [3]. However, the intense use of chemical fertilizers in the agricultural industry has unfortunately come at a significant environmental cost.

The impact of agriculture on surface and groundwater is often determined as negative due to the excessive release of nutrients like urea and phosphate into these water sources. Multiple farming activities such as livestock breeding, pesticide usage, fertilization and unsustainable land use lead to water pollution. Agriculture pollutes water resources as a result of the use of agrochemicals, organic substances and saltwater drainage [4]. The release of urea in agriculture is influenced by factors such as soil moisture, temperature, erosion, runoff and management practices. It is closely related to the phenomenon of nutrient runoff, which refers to the movement of fertilizers or nutrient-rich substances from agricultural fields into water bodies such as rivers, lakes and oceans [5]. The discharge of urea fertilizers in agriculture has major effects on both open and closed wastewater systems. Nutrient runoff in open water is governed by elements including hydrolysis, leaching and surface runoff, whereas in closed systems, runoff, erosion and restricted water circulation are the main driving forces [6]. This could help to create focused strategies to reduce nutrient runoff and protect the ecological integrity of essential aquatic ecosystems by understanding the processes at play and their impacts on open and closed water bodies.

When urea is hydrolysed in the soil, it causes the ammonium ions and nitrate to be susceptible to leaching and runoff. Excessive rainfall or irrigation can cause the movement of these nitrogen compounds through the soil profile and into groundwater or nearby water bodies, contributing to nutrient pollution [7]. The presence of water triggers the hydrolysis process, where it moves downwards through the soil profile and potentially reaches groundwater sources. Additionally, high temperatures and pH levels can increase the activity of urease enzymes which promotes faster hydrolysis and the subsequent release of ammonium ions [6]. A previous study has shown that increasing the temperature from 20 °C to 40 °C positively affect the urea removal process [8]. Another study highlighted that adjusting the pH level during the adsorption process notably enhanced removal efficiency [9]. The dissolved nitrate may also be carried away by runoff and enter water bodies; this can disrupt aquatic ecosystems, leading to oxygen depletion, harmful algal blooms, fish kills and imbalances in the food chain [10].

Studies have shown that urea ($CO(NH_2)_2$) is the most common waste in the agricultural, pharmaceutical and textile industries that contributes to water quality pollution [11]. Urea is a common fertilizer that plays a crucial role in providing plants with the essential nutrient, nitrogen. When in aqueous solutions with ammonium nitrate or magnesium sulphate, it can also be applied as a foliar fertilizer [12]. Urea is a high-nitrogen content fertilizer, typically containing around 46 % nitrogen by weight [13]. It can be found in various types of fertilizers, as tabulated in Table 1. Urea fertilizers are the most concentrated solid nitrogen fertilizer which contains 46 % N [14], while polymer-coated urea contains 43 % N, sulfur-coated urea contains 37 % N, urea formaldehyde contains 18 % N [15] and urea-ammonium nitrate contains 32 % N [16]. These fertilizers contain urea as a source of nitrogen, either as the primary nitrogen component or as part of a balanced nutrient blend.

Table 1. Types of fertilizers containing urea.

Type of fertilizer	Urea content (%)	Composition	Reference
Urea fertilizer	46	-	[14]
Polymer-coated urea	43	Polymer wrapped with urea for 60 days	[17]
Sulfur-coated urea	37	Sulfur wrapped with urea for 60 days	[17]
Urea formaldehyde	18	Polycondensation reaction of urea and formaldehyde	[17]
Urea-ammonium nitrate	32	-	[16]

- : No data reported.

Since utilization of urea is common in agriculture, leaching and nutrient runoff is also a common problem, leading to eutrophication and soil acidification. Consequently, a study found that 60 % of cropland areas had elevated N readings [18]. Another study also found elevated nitrate levels in ground water from agro-ecosystems (4.1 ± 0.33 mg/L) compared to the levels in ground water from forest ecosystems (0.5 ± 0.04 mg/L) [19]. Furthermore, excessive long term urea fertilization was found to reduce fertility and diversity in soil microbiomes [20]–[22]. Long term urea usage may increase soil pH, which can affect biological processes in the ecosystem [23]. However, a bigger problem is the waste generated during urea production. Urea plants release wastewater with ammonium and urea levels ranging from 20-230 ppm (10–610 $g/t_{product}$) and 20–320 ppm (10–840 $g/t_{product}$), respectively [24]. During the production process, the vaporization of water entrains droplets of urea solution, which can then pass into the condensate [25] that can seep from the urea plant along with wastewater. Urea enters the environment not only with wastewater from production plants but also by leaching from fields and agro-breeding farms that use it as a raw material. Treatment methods for this wastewater include hydrolysis, enzymatic hydrolysis, adsorption, electrochemical oxidation, and certain decomposition pathways: i) biological bed, ii) strong oxidants and iii) catalytic decomposition [12].

This study focused on adsorption as a treatment method for urea wastewater. Adsorption has a wide range of applications including the treatment of water and wastewater, air purification, gas separation and the elimination of toxins or pollutants from different industrial processes [26]. It is also used in the removal of low concentrations of non-degradable organic compounds from groundwater, drinking water, and processed water, or as a tertiary cleansing process. Adsorption is also one of the most extensively studied processes as a treatment for wastewater containing urea [25]. Adsorption is a surface-based process in which molecules or particles from a fluid phase adhere to the surface of a solid or liquid material, called the adsorbent [27]. An adsorbent is a solid material used for the adsorption process while an adsorbate is any substance that has undergone adsorption at the surface during the adsorption phase [28]. The adsorbate molecules or particles accumulate on the surface of the adsorbent through various intermolecular forces or chemical bonding. It occurs when the attractive forces between the adsorbate and the adsorbent are stronger than the forces holding the adsorbate in the fluid phase [29]. The effectiveness of adsorption is also influenced by process variables like temperature, pressure and contact time [30].

The adsorption process can be categorized into chemical adsorption and physical adsorption with each process having its own characteristics. Physical adsorption or physisorption, involves nonspecific weak van der Waals forces including dipole moments, polarization forces, dispersive forces, short-range repulsive interactions with activation energies [31], or a distance-dependent interaction between atoms or molecules [29] by forming a multimolecular layer. Physisorption can happen at low temperatures, and the surface area of the adsorbent plays an important role [32]. The process is reversible, and desorption can occur by increasing the temperature or decreasing the pressure [33]. In contrast, chemical adsorption or chemisorption is a highly specific, non-reversible, comparatively slower process that involves the formation of stronger covalent or coordinated chemical bonds with specific functional groups or metal ions [34]. It happens when the adsorbate molecules are held on the adsorbent surface unimolecular layer by chemical forces with the electrons being shared [35]. The adsorption rate increases with temperature and adsorbent surface area [36]. In addition, ion exchange, surface complexation and physical encapsulation are additional mechanisms that contribute to adsorption. Understanding the precise interactions at play enables the selection of a suitable adsorbent material and the optimisation of process parameters to ensure effective adsorption.

Among the possible water treatment techniques, adsorption by solid sorbents shows potential as one of the most efficient methods for the treatment and removal of contaminants in wastewater treatment. Adsorption systems are generally easier to operate and require less maintenance compared to some chemical or biological treatment processes. They do not rely on complex chemical reactions or biological activity, making them relatively stable and robust. Adsorption has advantages over other methods because of its straightforward experimental design that involves a low investment in terms of both the initial cost and land required. Locally available natural materials, agricultural waste and industrial waste can be utilized as low-cost adsorbents. Utilizing waste materials as a source for producing solid sorbents is an environmentally sustainable approach that can help address both waste management and resource scarcity issues. A common material used as a solid sorbent is activated carbon. This material is a good adsorbent as it has a wide spectrum of functional groups on the surface, high surface area, large porosity, and a well-developed internal pore structure [37]. In the carbon structure, the main functional groups responsible for the uptake of pollutants are carboxyl, carbonyl, phenols, lactones, quinones and others [38]. Functional groups have a major influence on the unique adsorption properties of activated carbon. Besides activated carbon, other adsorbent materials include natural or synthetic zeolites, natural clay minerals, silica gel and activated aluminium, as well as silicic acid [39].

Solid sorbents from waste materials can be divided into organic and inorganic materials. The organic materials are from biomass, agricultural waste, food waste and polymers [40], whereas

inorganic materials are mainly from industrial waste such as silicate, fly ash, wood, and scrap lumber [41]. These wastes have been reported as adsorbents for various adsorbates, as shown in Table 2. Oxidized starch nanoparticles, oil palm activated carbon fibres and activated alumina were found to be efficient in removing urea [42]. Oxidized starch nanoparticles showed a promising adsorption capacity of 185.2 mg/g and a high removal percentage of 95 % in a relatively short period of 4 hours [43]. The next promising adsorbent was activated carbon fibres (ACF) from oil palm. A study found that electronegative OH groups on the adsorbent surface in the alkaline urea solution caused ionic repulsion towards partially anionic urea. The strength of this ionic repulsion increased with increasing OH functional groups on the ACF surface [44]. The urea concentration was efficient, with 8.162 mg/L at 165 °C after 120 min, which was below the effluent standard. Next, activated alumina was compared with activated carbon for the removal of urea from wastewater. The maximum adsorption capacities at pH 9.0 were 24 % and 31 % for granular activated alumina and granular activated carbon, respectively, [45]. Fly ash and sweet potato peels were found to be more efficient in removing heavy metal contaminants. Fly ash was found to adsorb urea as much as 97.5 % at 20 mg/L of Cd at 25 °C [46], while sweet potato peels removed 95 % in 10 mg/L of Pb (II) at the same temperature [47]. Activated carbon from molasses was found to be efficient in removing dyes in wastewater. Activated carbon derived from cocoa removed 98 % of contaminants in a 4 mg/L concentration of dye at 25 °C [48].

This study takes a novel approach by utilizing a solid sorbent derived from industrial solid waste of the photovoltaic industry, specifically alkaline sludge, to remove urea from aqueous solutions. Alkaline sludge, a byproduct of the photovoltaic industry, offers significant potential as a starting material for a new and sustainable process [50]. While conventional adsorbents like activated carbon and agricultural byproducts have been extensively studied, the use of photovoltaic industry waste as an adsorbent remains largely unexplored. This work also emphasizes reducing industrial solid waste by repurposing it as an effective adsorbent, addressing both waste management challenges and water pollution. Solid adsorbents, including those derived from industrial waste, are known for their efficiency in treating and removing organic contaminants [51]. By focusing on the feasibility and efficiency of utilizing alkaline sludge, this study not only provides an innovative method for urea removal, but also presents a sustainable and cost-efficient solution for managing waste from the rapidly expanding photovoltaic industry. Ultimately, this approach contributes to addressing environmental concerns related to both solid waste and water contamination.

Table 2. Solid sorbents from waste materials.

Material	Initial concentration	pH	Temperature (°C)	Removal Percentage (%)	Reference
Oxidized Starch nanoparticles	1500 mg/L of urea	9	25	95	[42]
Oil Palm Activated Carbon Fibers (ACF)	8.162 mg/L of urea	-	165	84.7	[44]
Granular activated alumina	1000 mg/l of urea	9	25	24	[45]
Granular activated carbon	1000 mg/l of urea	9	25	31	[45]
Coal Fly ash	20 mg/L of cadmium (Cd) in urea	7	25	82	[46]
Activated Carbon from Cocoa	4 mg/L of Iron(II)	-	25	98	[48]
Sweet Potato Peels	10 mg/L of Lead(II)	7	25	95	[47]
Silica Gel	15 mg/L of nitrate (NO_3^-)	7	20	87	[49]
Calcined Alkaline Sludge	30 mg/l of urea	-	60	85	This study

- : No results reported.

EXPERIMENTAL

Chemicals and Materials

Urea was purchased from Chemiz, Malaysia, while the alkaline sludge (AS) was obtained from a photovoltaic industry site in Sarawak, Malaysia.

Methods

Preparation of Adsorbents

The AS was dried in an oven at a temperature of 110 °C for 24 hours to remove moisture. After it had completely dried, the AS sample was ground in a mortar and stored in a closed container. This was denoted as dried alkaline sludge (DAS). For the calcined alkaline sludge (CAS), the DAS was calcined at a temperature of 900 °C for 3 hours with a ramp rate of 10 °C/min. After being calcined, the sample was ground and stored in a closed container. Calcination was performed to remove volatile compounds from the sludge [52].

Characterization

The adsorbents were characterized using X-ray Diffraction (XRD) using a Bruker AXS D8 Advance instrument. All the diffractograms were matched with data from the International Centre for Diffraction Data (ICDD) to identify the chemical composition of the samples. N_2 adsorption-desorption isotherms were obtained from a gas sorption analyser, Micromeritics Tristar II Plus. The isotherms were used to calculate surface areas by the Brunauer, Emmet and Teller (BET) method. The pore volume and average pore diameter values were obtained by the Barrett, Joyner and Halenda (BJH) method. The mesopore and micropore surface areas were determined using the t-plot method. The mesopore surface area corresponded to the external surface area [53]. The pore size distribution was computed using the BJH method. The analysis began with degassing of the adsorbent at 150 °C under vacuum for 6 hours, followed by analysis under circulated liquid N_2. The surface functional groups of the adsorbents were obtained using a Perkin Elmer FTIR spectrometer by the attenuated total reflectance (ATR) method. The adsorbed urea was measured using a thermogravimetric analyzer (TGA) from Mettler Toledo.

Urea Removal Study

The urea removal study was performed using several parameters by batch adsorption. Each experiment was conducted according to specified parameters such as type of adsorbent, initial concentration, adsorbent loading, time of adsorption and adsorption temperature. This experiment was repeated to obtain the most efficient adsorbent and adsorption parameters for urea adsorption.

The maximum wavelength absorption for the urea solution at 50 mg/L was obtained using ultraviolet-visible (UV-Vis) spectrometry (UV5Nano UV-Vis Spectrometer, Mettler Toledo) at 204 nm [54]. A series of urea solutions at different concentrations was prepared to obtain a linear regression equation that was used to determine the urea solution concentration after the adsorption process. The adsorption capacity (Equation 1) and removal percentage (Equation 2) were calculated according to the following formulae:

$$\left(\frac{C_0 - C_1}{m}\right) \times V \qquad \text{Equation 1}$$

$$\left(\frac{C_0 - C_1}{C_0}\right) \times 100\% \qquad \text{Equation 2}$$

where C_0 is the initial concentration (mg/L) of urea solution, C_1 is the final concentration (mg/L) of urea solution after the adsorption process, V is the volume of urea solution (mL), and m is the mass of adsorbent (g) used throughout the experiments.

The batch adsorption was conducted using DAS and CAS adsorbents with a urea concentration of 50 mg/L, adsorbent dosage of 0.2 g, 6 hours of adsorption time and an adsorption temperature of 28 °C. Based on the outcome of these experiments using CAS and DAS, the most efficient adsorbent was used to determine the next parameter. The batch adsorption was conducted using several parameters such as initial concentration (30, 50 and 70 mg/L), adsorbent dosage (0.2, 0.4 and 0.6 g), adsorption temperature (28, 35 and 40 °C) and adsorption time (4, 6 and 8 hours). The adsorbent was chosen using the most efficient urea adsorption conditions to study the urea interaction using XRD, FTIR and TGA analyses.

RESULTS AND DISCUSSION

Characterization

Results of the XRD analysis of the adsorbents are shown in Figure 1. The DAS diffractogram was dominated by the rhombohedral phase of $CaCO_3$ (ICDD file 01-081-2027) with lattice parameters of a=4.9910 Å, b=4.9910 Å and c=17.0620 Å. The sharp peak at 2θ=29.44° was the most intense before and after calcination, indicating that CAS was still monopolized by $CaCO_3$ and $CaSiO_3$. CAS exhibited the $CaCO_3$ (ICDD file 01-086-0174) rhombohedral phase with lattice parameters of a=4.9880 Å, b=4.9880 Å and c=17.0680 Å, as well as the monoclinic $CaSiO_3$ (ICDD file 01-075-1396) phase at lattice parameters of a=15.4090 Å, b=7.3220 Å and c=7.0630 Å. The higher intensity of $CaSiO_3$ after calcination at 900 °C indicates the formation of $CaSiO_3$ from $CaCO_3$, as shown in Equation 3. The presence of the crystalline tetragonal SiO_2 peak after calcination matched with the ICDD file 01-076-0941 with lattice parameters of a=4.9984 crystalline Å, b=4.9984 Å and c=7.0242 Å.

This may be due to the remaining unreacted SiO_2 after the calcination process. In addition, the presence of carbonate compounds on the DAS surface may have prevented the detection of SiO_2.

$$CaCO_3 + SiO_2 \rightarrow CaSiO_3 + CO_2 \qquad \text{Equation 3}$$

Based on the N_2 adsorption-desorption isotherms in Figure 2, DAS showed a Type IV isotherm, according to the International Union of Pure and Applied Chemistry (IUPAC) definition [55]. This isotherm is common for mesoporous adsorbents, which are identified by adsorptive interactions and the interactions between molecules in the condensed state. The knee shape at a relative pressure of around 0.03 indicates that monolayer adsorption was complete, and followed by multilayer adsorption. After calcination, the isotherm for CAS changed to a Type II isotherm with the same path as Type IV, but an unrestricted monolayer-multilayer adsorption up to high relative pressure. DAS exhibited a higher quantity of N_2 adsorbed, consistent with its higher surface area. Both of the hysteresis loops were classified as Type H3 hysteresis given by non-rigid aggregates of plate-like particles, and the pore network consisted of macropores that were not completely filled with pore condensate [55]. It is noteworthy to observe that the hysteresis loop for DAS was broader compared to CAS; this is associated with greater mesopore structure [56]. CAS also exhibited a significant amount of N_2 adsorption, but this was less than that of DAS, consistent with its lower surface area. The pore size distribution curves that were computed using the BJH method indicate that the DAS predominantly contained smaller mesopores compared to CAS (Figure 3). The calcination process resulted in the carbonate form of DAS being decomposed and agglomerated. Hence, the pore size distribution curve for CAS shifted towards a larger pore size. Although the distribution for CAS appeared sharper and more intense than that of DAS, DAS nonetheless had a broader distribution at the smaller mesopore region of 2-50 nm [57].

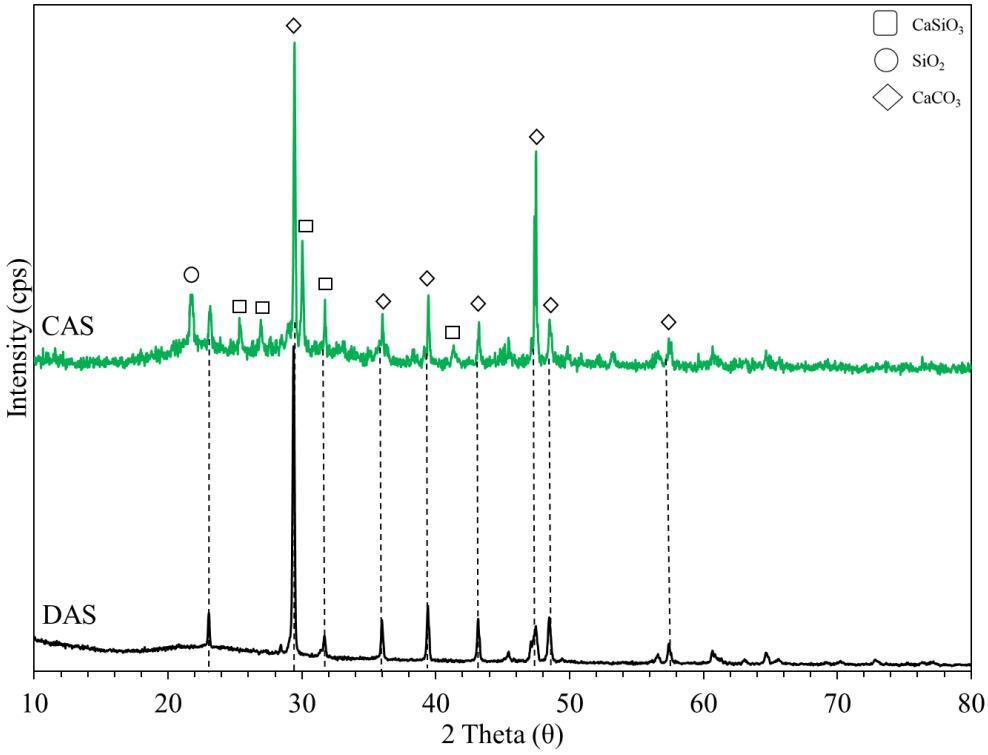

Figure 1. XRD patterns for DAS and CAS.

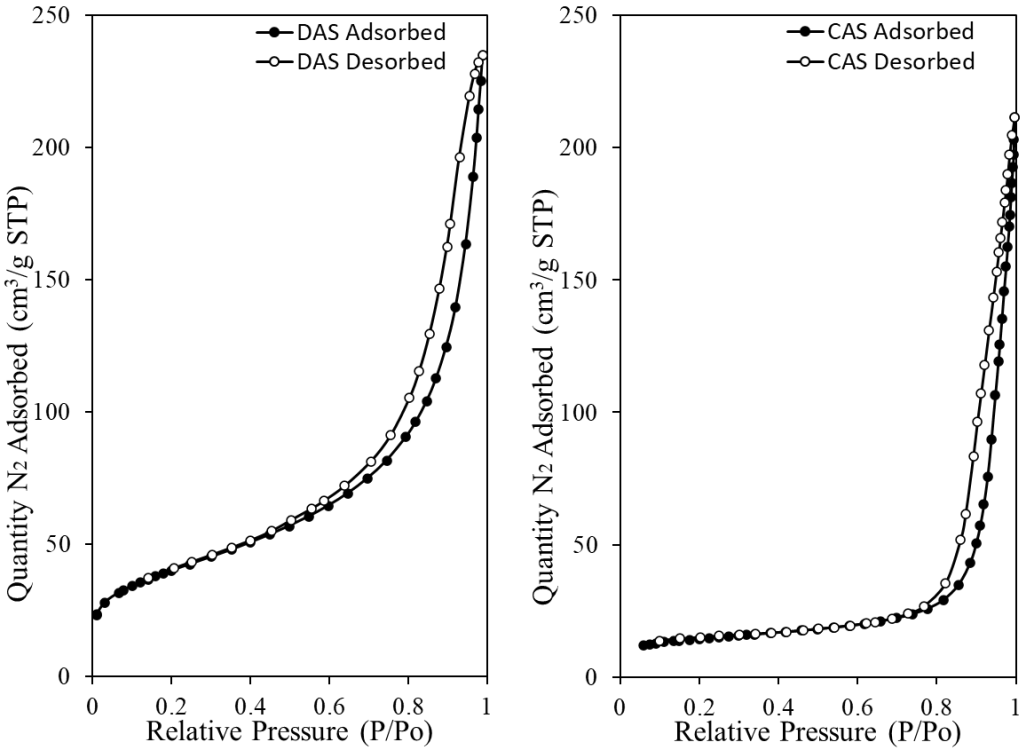

Figure 2. N_2 adsorption-desorption isotherms of the adsorbents.

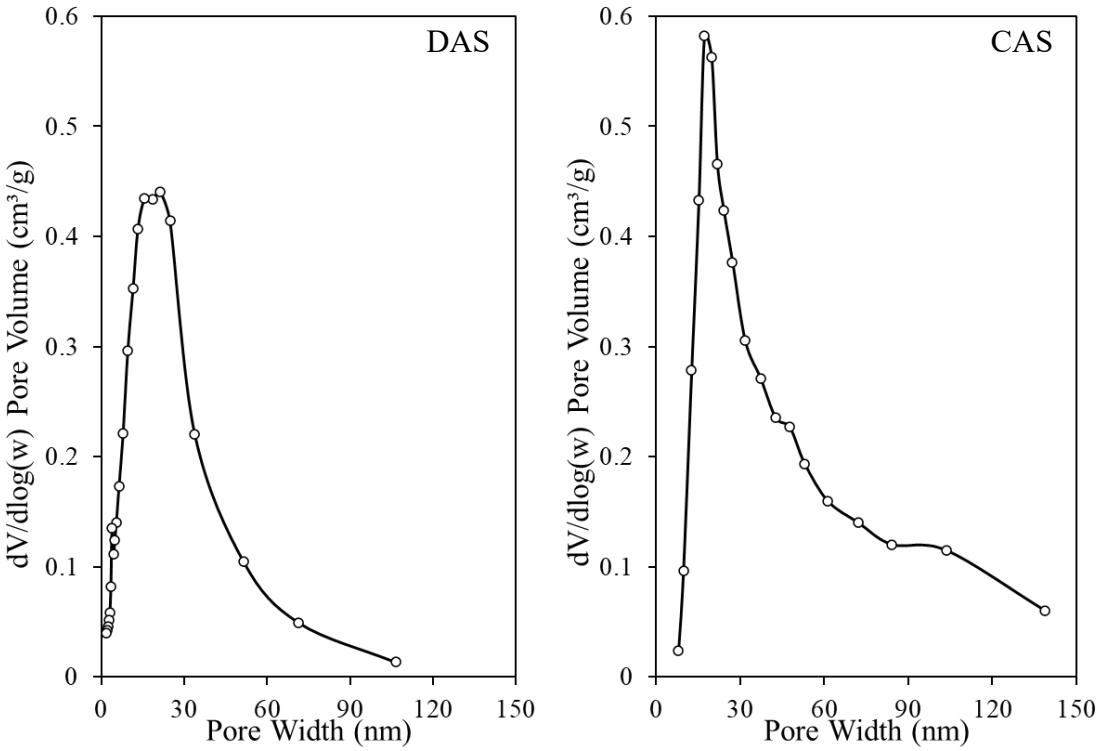

Figure 3. Pore size distribution of the adsorbents.

Table 3. Textural properties of the adsorbents.

Adsorbents	BET Surface Area (m^2/g)	Mesopore Surface Area (m^2/g)	Micropore Surface Area (m^2/g)	Pore Volume (cm^3/g)	Micropore Volume (cm^3/g)	Average Pore Diameter (nm)
DAS	144.30	129.25	15.04	0.3531	0.00542	10.98
CAS	52.81	31.28	21.53	0.3151	0.00859	23.10

Based on the textural properties in Table 3, DAS exhibited a significantly high BET surface area (144.30 m^2/g) compared to CAS (52.81 m^2/g). The pore volume was consistent with the BET surface area, where DAS had a higher value than CAS. Both DAS and CAS showed mesopore surface area values higher than micropore surface area values. However, the calcination process enhanced the micropore surface area (21.53 m^2/g) of CAS nearly as much as its mesopore surface area (31.28 m^2/g). In contrast, the micropore surface area of DAS was significantly low compared to its mesopore surface area. These results are consistent with the micropore volume of CAS being higher than that of DAS. Therefore, it is worth noting that the carbonate form of DAS contributed to its mesopore surface area. In addition, the calcination process causing particle agglomeration was supported by the average pore diameter of CAS being larger (23.10 nm) than that of DAS (10.97 nm). Although the calcination process was found to be efficient in pore structure formation, it had a tendency to aggregate particles and generate larger pores.

FTIR analysis was used to characterize the surface functional groups of the adsorbents. Figure 4 shows the FTIR spectra, while peak assignments are listed in Table 4. Both the DAS and CAS spectra showed fingerprint bands at 710 and 873 cm^{-1}, corresponding to Ca-O and Ca-O-Ca bonding, respectively [58]. Another absorption band that indicates the presence of CaO at 1415 cm^{-1} [58] was not observed due to overlap with the bicarbonate signal. SiO_2 was detected by the presence of vibrational modes for Si-O-Si symmetric stretching at 790 cm^{-1} [59], as well as Si-O-Si asymmetric stretching at 1025 and 1060 cm^{-1} [57–59]. After calcination, the formation of $CaSiO_3$ was detected through the Ca-O-Si bond stretch at 920 cm^{-1} [60,61]. As the XRD pattern detected the carbonate forms of DAS and CAS, the absorption band for Si-C stretching at 790 cm^{-1} [62,63] may have overlapped with Si-O-Si symmetric stretching. This is supported by the lower intensity peak for CAS compared to DAS, due to the dissociation of carbonate after calcination. Various carbonate species were detected at 1300 to 1600 cm^{-1} for both CAS and DAS. The bands at 1413 and 1645 cm^{-1} were assigned to symmetric and asymmetric O-C-O stretching of bicarbonate, respectively [53]. The shoulder peak at 1506 cm^{-1} corresponded with the asymmetric O-C-O stretch of monodentate carbonate, while the absorption bands at 1338 and 1538 cm^{-1} were associated with the symmetric and asymmetric O-C-O stretching of bidentate carbonate, respectively [65]. A weak absorption band at 2349 cm^{-1} was assigned to the physisorbed CO_2, as the XRD pattern showed the carbonate compound. The broad peak at 3417 cm^{-1} was associated with O-H or Si-O-H stretching [58]. The presence of an OH group is consistent with the formation of bicarbonates [65] in DAS and CAS.

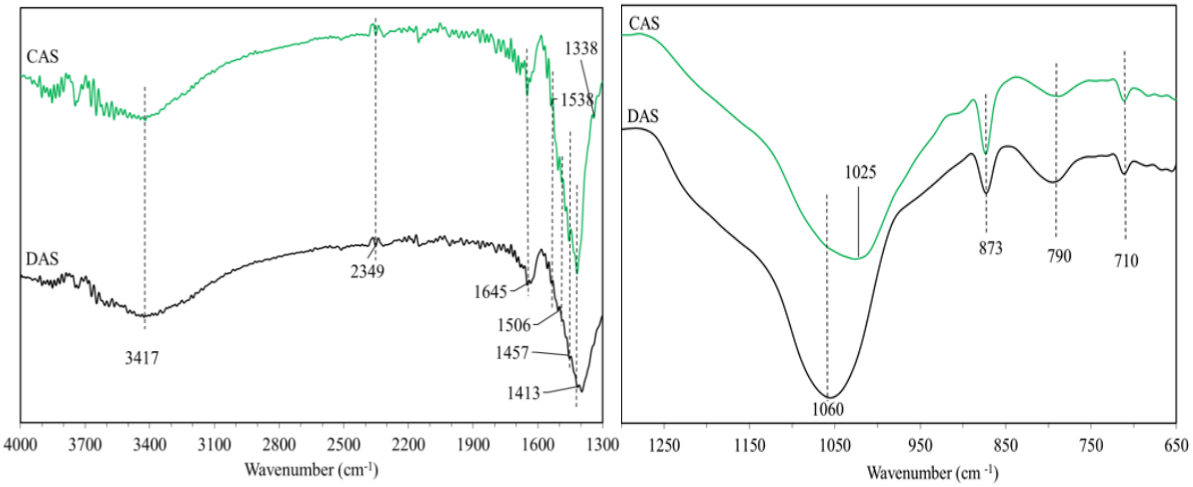

Figure 4. FTIR spectra for DAS and CAS.

Table 4. Vibrational frequencies in FTIR spectra.

Vibrational mode assignments	Experimental frequencies (cm^{-1})	Reported frequencies (cm^{-1})	References
Ca-O bond	710	710	[58]
Si-O-Si symmetric stretch	790	790	[59]
Si-C stretch	790	770-800, 790	[63], [66]
Ca-O-Si	920	1100-850/ 933.42 904.49, 890.99	[61], [62]
Ca-O-Ca	873	872	[58]
Si-O-Si asymmetric stretch	1025, 1060	1023/ 1050/ 1090	[57–59]
CaO	1413	1415	[58]
Bicarbonate			
Symmetric O-C-O stretch of bicarbonate	1413	1396-1500	[53]
Asymmetric O-C-O stretch	1645	1555-1720	[53]
Monodentate carbonate			
Asymmetric O-C-O stretch	1506	1446-1590	[67]
Bidentate carbonate			
Symmetric O-C-O stretch	1338	1243-1355	[67]
Asymmetric O-C-O stretch	1538	1535-1670	[67]
Physisorbed CO_2	2349	2347	[68]
OH or Si-O-H stretch	3417	3200-3500	[58]

Urea Removal Study

The two adsorbents, DAS and CAS, were tested in the urea removal study using 0.2 g of adsorbent, an initial concentration of 30 mg/L, and 6 hours of adsorption time at 28 °C. The removal percentage and adsorption capacity of CAS was found to be higher than that of DAS, as shown in Figure 5. This indicates that CAS was more effective in removing urea, with a removal percentage of 78.96 %, compared to DAS, which had only 45.63 %. The adsorption capacity of CAS was recorded at 4.54 mg/g, which was higher than that of DAS, at 3.54 mg/g. The calcination process of CAS enlarged the pore diameter, which provided more adsorption centres for the adsorbate in the solution. Hence, CAS was used for the investigation of the initial concentration.

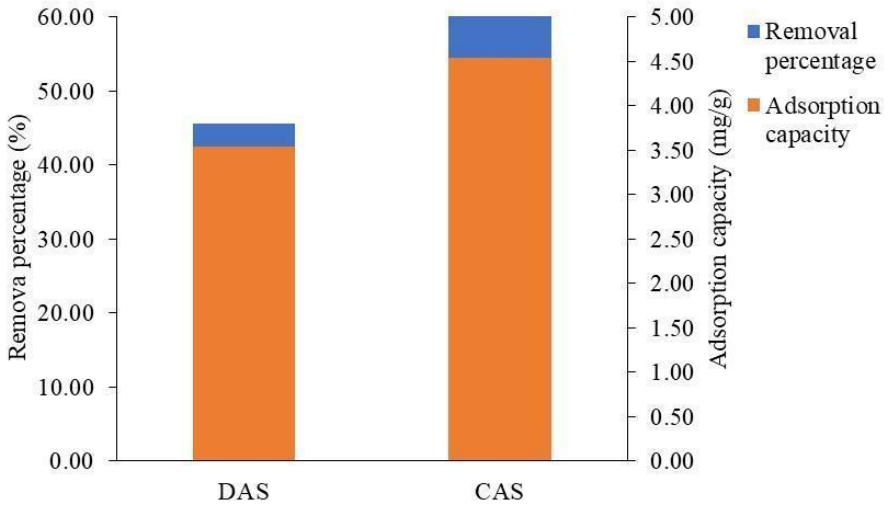

Figure 5. The effect of adsorbents (0.2 g adsorbent at an initial concentration of 30 mg/L for 6 hours of adsorption time at 28 °C).

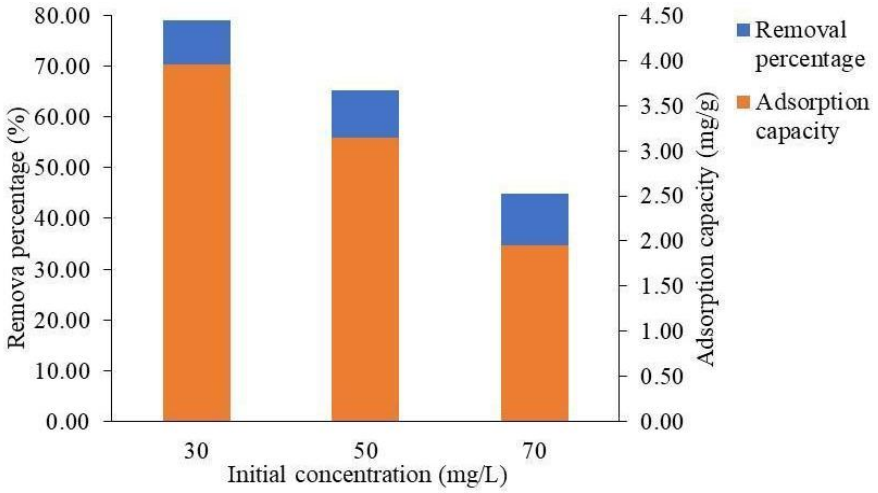

Figure 6. The effect of initial concentration (0.2 g of CAS for 6 hours of adsorption time at 28 °C).

Effect of Initial Concentration

The initial concentration may affect the removal of urea from aqueous solution. An increase in the initial concentration increases the probability of collisions between urea and adsorbent molecules [69]. This effect was investigated using three different initial concentrations: 30, 50 and 70 mg/L. Other parameters were fixed, with 0.2 g of CAS, and an adsorption time of 6 hours at 28 °C. The results in Figure 6 show that the initial concentrations were inversely proportional to the removal percentage. The lowest concentration of 30 mg/L exhibited the highest removal percentage of 79.13 % and adsorption capacity of 3.96 mg/g. This result was due to the availability of more adsorption binding sites at the initial stage [70]. A high initial concentration may also result in limited adsorption sites on the adsorbent. Therefore, an initial concentration of 30 mg/L was applied to investigate the next parameter, adsorbent dosage.

Effect of Adsorbent Dosage

The adsorbent dosage is a crucial factor in the process of urea removal from aqueous solution as it affects the amount of urea adsorbed per unit mass of the adsorbent [71]. To determine the most efficient adsorbent dosage, varying amounts of CAS were used at an initial concentration of 30 mg/L and a temperature of 28 °C. The dosages used were 0.2, 0.4 and 0.6 g. The outcome of the experiment, as shown in Figure 7, indicates that an adsorbent dosage of 0.2 g was the most efficient, with a removal percentage of 76.88 % and an adsorption capacity of 3.71 mg/g. CAS was well-dispersed in the aqueous urea solution, which led to better interactions at the adsorption site. Therefore, the significantly low removal percentage for the highest adsorbent dosage of 0.6 g may be due to CAS having a tendency to agglomerate, which reduced adsorption performance.

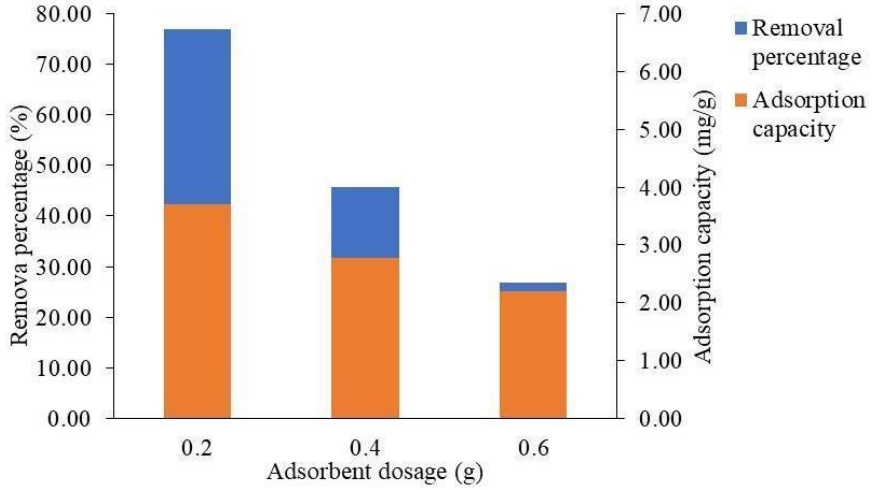

Figure 7. The effect of CAS adsorbent dosage (initial concentration of 30 mg/L for 6 hours adsorption time at ambient temperature).

Effect of Adsorption Temperature

The effect of temperature on the removal of urea from aqueous solution was investigated at 28, 35, and 40 °C. The results exhibited that the most efficient adsorption temperature was 40 °C. At this temperature, the aqueous solution dried out before 6 hours. Efficient adsorption at this temperature may be due to the faster diffusion and mixing of urea [72], or a higher number of molecules with a kinetic energy greater than the activation energy of the reaction. Some previous studies reported 22 % lower urea removal at 25 °C than 37 °C [73], whereas others found that complete urea removal only occurred at above 55 °C [72]. Therefore, the urea solution at 40 °C had the highest removal percentage of 80.56 % and adsorption capacity of 4.03 mg/g, as shown in Figure 8. Meanwhile, the removal percentage of urea at 35 °C indicated a significant difference of about 57.88 %, with an adsorption capacity of 2.893 mg/g. The adsorption temperature of 28 °C had slightly lower results, with a removal percentage of 55.38 % and an adsorption capacity of 2.768 mg/g. Thus, 40 °C was the most efficient adsorption temperature.

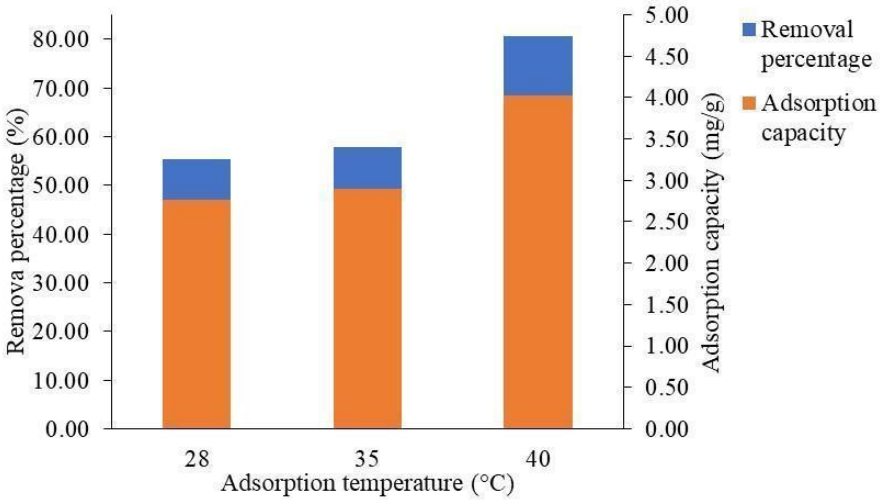

Figure 8. The effect of adsorption temperature (0.2 g of CAS at an initial concentration of 30 mg/L for 6 hours of adsorption time).

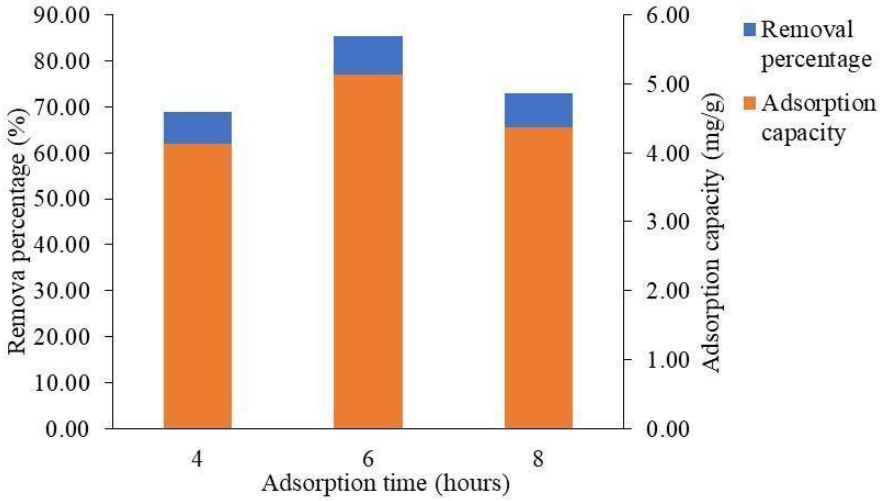

Figure 9. The effect of adsorption time (0.2 g CAS at an initial concentration of 30 mg/L and adsorption temperature of 40 °C).

Effect of Adsorption Time

This study also investigated the effect of adsorption time for urea removal by carrying out the adsorption process at 4, 6 and 8 hours. The results in Figure 9 show that 6 hours was the most efficient time for the adsorption process. The removal percentage at 6 hours was 85.42 %, with other parameters fixed (0.2 g CAS with an initial concentration of 30 mg/L at 40 °C). The adsorption capacity of urea at 6 hours was the highest, at 5.13 mg/g. The removal percentage decreased after the optimum time of 6 hours. This was due to the adsorbent being saturated with urea ions, thus releasing urea back into the solution [61].

Urea Interaction Study

After urea adsorption, the XRD pattern in Figure 10 showed that the $CaSiO_3$ peaks were diminished for CAS_UREA. The SiO_2 peak was less intense compared to that of CAS. Partial removal of the carbonate species from the calcination process generated active sites from SiO_2 and $CaSiO_3$ that could facilitate urea adsorption. Other comparable materials for urea adsorption include SBA-15 [74] and zeolite [75].

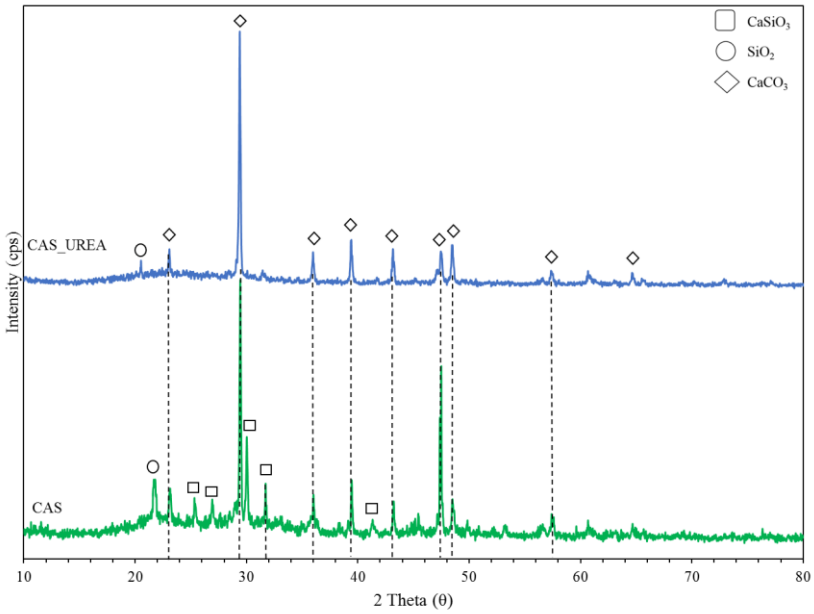

Figure 10. XRD patterns for CAS_UREA and CAS.

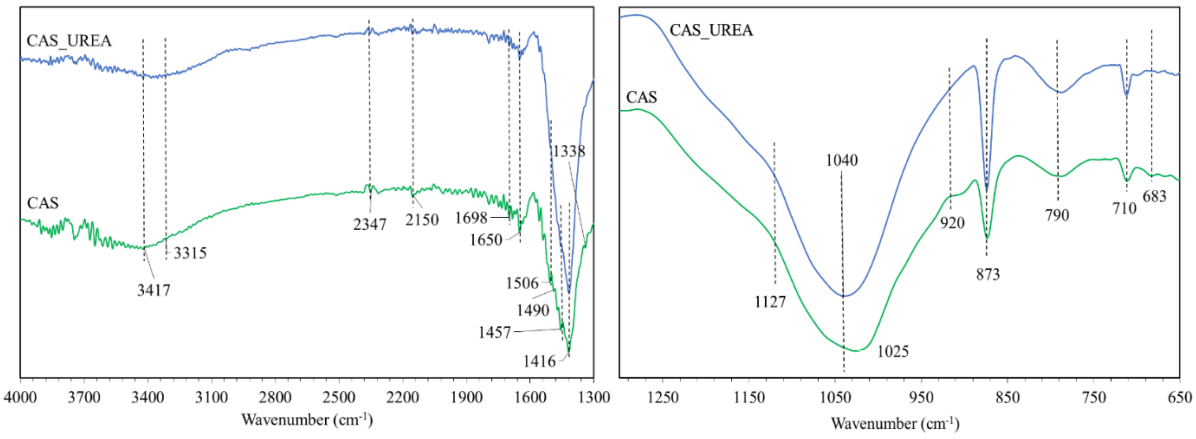

Figure 11. FTIR spectra of DAS and CAS.

Table 5. Vibrational frequencies for FTIR spectra.

Vibrational mode assignments	Experimental frequencies (cm^{-1})	Reported frequencies (cm^{-1})	References
Si-C	790	770-800, 790	[62,65]
SiC-N	1127	1126-1050	[76]
N-C-N stretch	1457	1455	[77]
NH bend	683	690	[77]
Symmetric NH_2 bend	1490	1490	[77]
NH_2 deformation	1650	1563-1631	[77]
Carbonyl of urea	1698	1660	[78]
Si-N	2150	2000-2200	[79]
N-H	3315	3350, 3310-3380	[76,78]

The surface interaction of urea with CAS was studied using FTIR analysis as shown in Figure 11, and the peak assignments are listed in Table 5. It was found that the higher intensity absorption band at 790 cm^{-1} corresponded to Si-C stretching due to the interaction of C from urea with Si from CAS. Further interactions between urea and CAS were observed in CAS_UREA, which had a wide shoulder peak at 1127 cm^{-1} corresponding to the SiC-N bond vibration [76]. The vibrational mode for asymmetric O-C-O stretching of a bicarbonate at 1650 cm^{-1} may have overlapped with the NH_2 deformation peak which is usually detected at 1563-1628 cm^{-1} [77]. A sharp shoulder peak at 1457 cm^{-1} was attributed to N-C-N stretching for urea, while another weak NH bending peak for urea was found at 690 cm^{-1} [77]. The small peak at 1698 cm^{-1} associated with carbonyl from urea [78] was less noticeable after urea adsorption possibly because of the adsorption of an NH group at another site. A small peak associated with Si-N at 2150 cm^{-1} indicated a minor interaction with urea [79]. The presence of O-H or Si-O-H stretching which occurs at a broad band around 3200-3500 cm^{-1} may have obscured the N-H peak that is usually detected at 3310-3380 cm^{-1} [76,78].

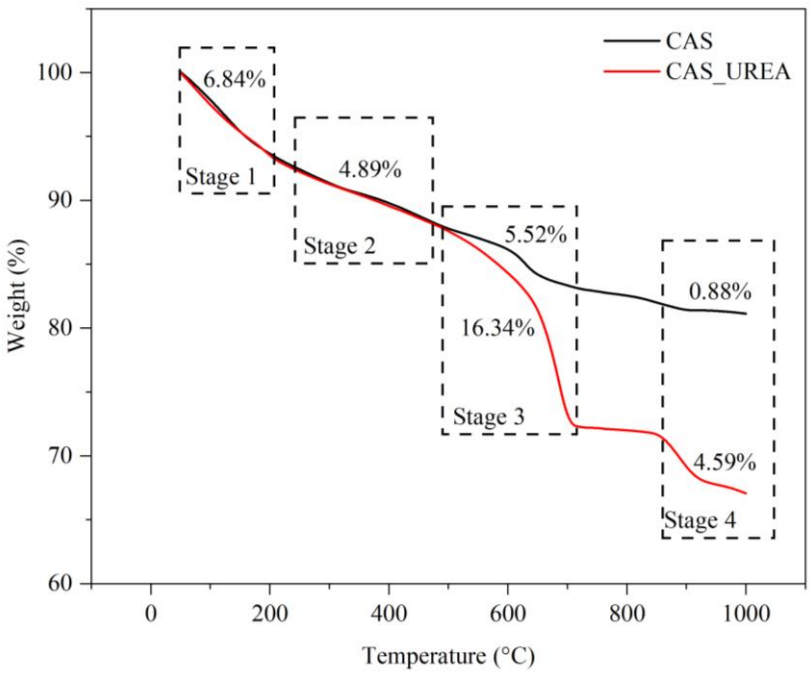

Figure 12. TGA curves of fresh and spent catalysts of urea interactions.

The adsorbed urea was measured using TGA analysis to study the different stages of urea interactions and weight loss. There were four stages of weight loss observed in the thermogram, as shown in Figure 12. The initial stage had a weight loss of 6.84 % at a temperature range of 50-200 °C, corresponding to the removal of water and evaporation of organic compounds at low boiling points [80]. The second weight loss appeared between 230-450 °C with a weight loss of about 4.89 %, perhaps from the decomposition of urea weakly bonded to carbonate species [81] and weakly bonded bicarbonates [82]. The third stage showed a significant weight loss with a 10.82 % difference between CAS_UREA and CAS. This loss occurred at 450 - 720 °C, indicating the decomposition of urea, suggesting interactions between urea and CAS. The TGA curve effectively illustrates the decomposition stages of the interactions between urea and CAS, thereby confirming such interactions [82,83]. This result also aligns with prior findings, where the final weight loss observed at 850 °C was associated with the decomposition of $CaCO_3$ to CaO [83,84]. The calcined CAS exhibited strong CO_2 affinity through carbonate formation and was supported by its decomposition at the final stage of weight loss.

CONCLUSION

This study addresses environmental issues caused by the growth of the agricultural sector, particularly the inadequate treatment of wastewater, by focusing on the reuse of industrial solid waste as an adsorbent for urea removal. Urea, commonly found in agricultural wastewater due to its use as a fertilizer, contributes to nutrient runoff problems. Alkaline sludge (AS) from photovoltaic industry waste was utilized as an adsorbent to address this issue. The AS sample was treated by drying and calcination to improve its adsorption properties. A lower BET surface area, primarily contributed by mesopore and micropore structures, did not negatively impact urea adsorption performance. Instead, the presence of SiO_2 and $CaSiO_3$ played a key role in urea removal. CAS, derived from calcined AS, showed the highest efficiency, achieving an 85.42 % removal percentage and an adsorption capacity of 5.13 mg/g with 0.2 g of adsorbent in a 30 mg/L urea solution for 6 hours at 40 °C. The interaction between urea and the adsorption sites, combined with the effect of temperature at 40 °C, enhanced the adsorption rate due to faster diffusion and the increased kinetic energy of the molecules. TGA analysis confirmed a 10.82 % weight loss due to urea adsorption, with evidence of Si-C and Si-N bond formation after adsorption. These findings demonstrate the potential of using photovoltaic industry waste for sustainable wastewater treatment, which offers a cost-effective and environmentally friendly solution.

ACKNOWLEDGEMENTS

The authors would like to express gratitude for the research grants awarded to Universiti Putra Malaysia by OCIM SDN. BHD (6300940), and by Universiti Putra Malaysia (9795800).

REFERENCES

1. Zeifman, L., Hertog, S., Kantorova, V. and Wilmoth, J. (2022) A world of 8 billion. *United Nations Dep. Econ. Soc. Aff.*, **140**, 140, 1–4.

2. Viana, C. M., Freire, D., Abrantes, P., Rocha, J. and Pereira, P. (2022) Agricultural land systems importance for supporting food security and sustainable development goals: A systematic review. *Sci. Total Environ.*, **806**.

3. Andrews, N., Sullivan, D. M., Julian, J. W. and Pool, K. E. (2011) Development and use of the OSU organic fertilizer and cover crop calculator. *Proc. West. Nutr. Manag. Conf.*, **9**, 61–66, January, 2011.

4. Stoyanova, Z. and Harizanova, H. (2019) Impact of agriculture on water pollution. *Agrofor*, **4**, 1.

5. Bijay-Singh and Craswell, E. (2021) Fertilizers and nitrate pollution of surface and ground water: an increasingly pervasive global problem. *SN Appl. Sci.*, **3**, 4, 1–24.

6. Wang, Y., *et al.* (2023) Zeolite reduces N leaching and runoff loss while increasing rice yields under alternate wetting and drying irrigation regime. *Agric. Water Manag.*, **277**, October, 2022.

7. Mateo-Sagasta, J., Zadeh, S. M., Turral, H. and Burke, J. (2017) Water Pollution from agriculture: A global review. *Food Agric. Organ.*, **1**, 1–35.

8. Rajakaruna, R. M. A. S. D., Sewwandi, B. G. N., Najim, M. M. M., Baig, M. B., Alotaibi, B. A. and Traore, A. (2023) Sustainable approaches for wastewater treatment: An analysis of sludge-based materials for heavy metal removal from wastewater by adsorption. *Sustain.*, **15**, 20.

9. Wang, G., Chi, T., Li, R., Li, T. and Zhang, X. (2024) Harnessing the rhizosphere sponge to smooth pH fluctuations and stabilize contaminant retention in biofiltration system. *Bioresour. Technol.*, **418**, December, 2024.

10. Beasley, V. R. (2020) Harmful algal blooms (Phycotoxins). In *Reference Module in Earth Systems and Environmental Sciences*, *Elsevier*, **2020**.

11. Kanu, O. K., Ijeoma and Achie (2011) Industrial effluents and their impact on water quality of receiving rivers in Nigeria. *J. Applieal Technol. Environ. Sanit.*, **1**, 1, 75–86.

12. Urbańczyk, E., Sowa, M. and Simka, W. (2016) urea removal from aqueous solutions—a review. *J. Appl. Electrochem.*, **46**, 10, 1011–1029.

13. Camberato, J. (2017) Improving the efficient use of urea-containing fertilizers. *Agron. Dep. Purdue Univ.*, 1–4.

14. Finch, H. J. S., Samuel, A. M., Lane, G. P. F. and Lockhart, J. A. R. (2014) Lockhart & Wiseman's crop husbandry including grassland. *Elsevier*.

15. Zhu, J., Su, Y., Chai, J., Muravev, V., Kosinov, N. and Hensen, E. J. M. (2020) Mechanism and nature of active sites for methanol synthesis from CO/CO_2 on Cu/CeO_2. *ACS Catal.*, **10**, 19, 11532–11544.

16. Ren, B., Guo, Y., Liu, P., Zhao, B. and Zhang, J. (2021) Effects of urea-ammonium nitrate solution on yield, N_2O Emission, and nitrogen efficiency of summer maize under integration of Water and Fertilizer. *Front. Plant Sci.*, **12**, 1–10, August, 2021.

17. Wu, Q., *et al.* (2021) Effects of different types of slow- and controlled-release fertilizers on rice yield. *J. Integr. Agric.*, **20**, 6, 1503–1514.

18. Shukla, S. and Saxena, A. (2019) Global Status of nitrate contamination in groundwater: Its occurrence, health Impacts, and mitigation Measures. *Handb. Environ. Mater. Manag.*, 869–888.

19. Zhang, X., Xu, Z., Sun, X., Dong, W. and Ballantine, D. (2013) Nitrate in shallow groundwater in typical agricultural and forest ecosystems in China, 2004-2010. *J. Environ. Sci. (China)*, **25**, 5, 1007–1014.

20. Ju, X. T., Kou, C. L., Christie, P., Dou, Z. X. and Zhang, F. S. (2007) Changes in the soil environment from excessive application of fertilizers and manures to two contrasting intensive cropping systems on the North China Plain. *Environ. Pollut.*, **145**, 2, 497–506.

21. Mandal, A., Patra, A. K., Singh, D., Swarup, A. and Ebhin Masto, R. (2007) Effect of long-term application of manure and fertilizer on biological and biochemical activities in soil during crop development stages. *Bioresour. Technol.*, **98**, 18, 3585–3592.

22. Sarathchandra, S. U., Ghani, A., Yeates, G. W., Burch, G. and Cox, N. R. (2001) Effect of nitrogen and phosphate fertilisers on microbial and nematode diversity in pasture soils. *Soil Biol. Biochem.*, **33**, 7–8, 953–964.

23. Motasim, A. M., *et al.* (2024) Urea application in soil: processes, losses, and alternatives—a review. *Discov. Agric.*, **2**, 1.

24. Matijašević, L., Dejanović, I. and Lisac, H. (2010) Treatment of wastewater generated by urea production. *Resour. Conserv. Recycl.*, **54**, 3, 149–154.

25. Weerakoon, D., *et al.* (2023) A critical review on current urea removal technologies from water: An approach for pollution prevention and resource recovery. *Separation and Purification Technology*, *Elsevier B.V.*, **314**, 01-Jun-2023.

26. Vishali, S. and Kavitha, E. (2021) Application of membrane-based hybrid process on paint industry wastewater treatment. In *Membrane-based Hybrid Processes for Wastewater Treatment*, *Elsevier*, 97–117.

27. Hu, H. and Xu, K. (2019) Physicochemical technologies for HRPs and risk control. In *High-Risk Pollutants in Wastewater*, *Elsevier*, 169–207.

28. Rao, S. N. (2018) Adsorption. *Interface Sci. Technol.*, **21**, 251–331, Jan. 2018.

29. Pourhakkak, P., Taghizadeh, A., Taghizadeh, M., Ghaedi, M. and Haghdoust, S. (2021) Fundamentals of adsorption technology. In *Interface Science and Technology Elsevier*, **33**, 1–70.

30. Sahoo, T. R. and Prelot, B. (2020) Adsorption processes for the removal of contaminants from wastewater: the perspective role of nanomaterials and nanotechnology. *Nanomater. Detect. Remov. Wastewater Pollut.*, 161–222, Jan. 2020.

31. Tao, J. and Rappe, A. M. (2014) Physical adsorption: Theory of van der Waals interactions between particles and clean surfaces. *Phys. Rev. Lett.*, **112**, 10, Mar. 2014.

32. Artioli, Y. (2008) Adsorption. *Encycl. Ecol. Five-Volume Set*, 1–5, 60–65, Jan. 2008.

33. Obulapuram, P. K., *et al.* (2021) Adsorption, equilibrium isotherm, and thermodynamic studies towards the removal of reactive orange 16 dye using Cu(I)-polyaninile composite. *Polym. 2021,* **13**, 20, 3490, Oct. 2021.

34. Xing, B. and Pignatello, J. J. (2004) Sorption - Organic Chemicals. In *Encyclopedia of Soils in the Environment, Elsevier*, **4**, 537–548.

35. Kwon, S., Fan, M., DaCosta, H. F. M., Russell, A. G., Berchtold, K. A. and Dubey, M. K. (2011) Chapter 10: CO_2 sorption. In *Coal Gasification and Its Applications*, *Elsevier*, 293–339.

36. Patterson, H. B. W. (2009) Chapter 2 - Adsorption. In *Bleaching and Purifying Fats and Oils: Theory and Practice*, *Elsevier Inc*., 97–151.

37. Ren, J., Wei, H. L., Xu, L. and Jia, L. Y. (2019) Blood detoxication. *Compr. Biotechnol.*, 723–734, Jan. 2019.

38. Forouzesh, M., Ebadi, A., Aghaeinejad-Meybodi, A. and Khoshbouy, R. (2019) Transformation of persulfate to free sulfate radical over granular activated carbon: Effect of acidic oxygen functional groups. *Chem. Eng. J.*, **374**, 965–974, Oct. 2019.

39. Saini, V. K. and Shankar, A. (2019) How to improve selectivity of a material for adsorptive separation applications. *Handb. Environ. Mater. Manag.*, 1469–1505.

40. Chavan, P., Sharma, P., Sharma, S. R., Mittal, T. C. and Jaiswal, A. K. (2022) Application of high-intensity ultrasound to improve food processing efficiency: A review. *Foods (Basel, Switzerland)*, **11**, 1, Jan. 2022.

41. Shalbafan, A., Welling, J. and Hasch, J. (2017) Effect of aluminosilicate powders on the applicability of innovative geopolymer binders for wood-based composites. *Eur. J. Wood Wood Prod.*, **75**, 6, 893–902, Nov. 2017.

42. Zaher, A. and Shehata, N. (2021) Recent advances and challenges in management of urea wastewater: A mini review. *IOP Conf. Ser. Mater. Sci. Eng.*, **1046**, 1, 012021, Feb. 2021.

43. Abidin, M. N. Z., *et al.* (2018) Highly adsorptive oxidized starch nanoparticles for efficient urea removal. *Carbohydr. Polym.*, **201**, 257–263, Dec. 2018.

44. Ooi, C. H., Cheah, W. K., Sim, Y. L., Pung, S. Y. and Yeoh, F. Y. (2017) Conversion and characterization of activated carbon fiber derived from palm empty fruit bunch waste and its kinetic study on urea adsorption. *J. Environ. Manage.*, **197**, 199–205, Jul. 2017.

45. Safwat, S. M. and Matta, M. E. (2018) Adsorption of urea onto granular activated alumina: A comparative study with granular activated carbon. *J. Dispers. Sci. Technol.*, **39**, 12, 1699–1709, Dec. 2018.

46. Zhang, Z., Wang, B. and Sun, Q. (2014) Fly ash-derived solid amine sorbents for CO_2 capture from flue gas. In *Energy Procedia*, **63**, 2367–2373.

47. Soliman, N. K. and Moustafa, A. F. (2020) Industrial solid waste for heavy metals adsorption features and challenges; a review. *J. Mater. Res. Technol.*, **9**, 5, 10235–10253, Sep. 2020.

48. Liza, A. Y. *et al.* (2022) Effect of activated carbon made from cocoa (Theobroma Cacao L.) shells on the adsorption of iron in aquifer water. *Chem. Eng. Trans.*, **96**, 499–504, Nov. 2022.

49. Shafqat, S. S., *et al.* (2019) Development of amino-functionalized silica nanoparticles for efficient and rapid removal of COD from pre-treated palm oil effluent. *J. Mater. Res. Technol.*, **8**, 1, 385–395, Jan. 2019.

50. Ngoc, U. N. and Schnitzer, H. (2009) Sustainable solutions for solid waste management in Southeast Asian countries. *Waste Manag.*, **29**, 6, 1982–1995, Jun. 2009.

51. Nageeb, M. (2013) Adsorption technique for the removal of organic pollutants from water and wastewater. In *Organic Pollutants - Monitoring, Risk and Treatment*, *IntechOpen*.

52. Mahutjane, T. C., Tchadjié, L. N. and Sithole, T. N. (2023) The feasibility of utilizing sewage sludge as a source of aluminosilicate to synthesise geopolymer cement. *J. Mater. Res. Technol.*, **25**, 3314–3323, Jul. 2023.

53. Hakim, A., Marliza, T. S., Abu Tahari, M. N., Yusop, M. R., Mohamed Hisham, M. W. and Yarmo, M. A. (2016) Development of α-Fe_2O_3 as adsorbent and its effect on CO_2 capture. *Mater. Sci. Forum*, **840**, 421–426.

54. Ooi Tee Ching and Ganesan, V. (2004) Tourism set to rake in RM30b in receipts. *New Straits Times*, **B1**, May-2004.

55. Thommes, M., *et al.* (2015) Physisorption of gases, with special reference to the evaluation of surface area and pore size distribution (IUPAC Technical Report). *Pure Appl. Chem.*, **87**, 9–10, 1051–1069.

56. Lahuri, A. H., *et al.* (2020) Comparative adsorption isotherm for beryllium oxide/ iron(III) oxide toward CO_2 adsorption and desorption studies.

Mater. Sci. Forum, *1010 MSF*, 361–366.

57. Lahuri, A. H., Adnan, R., Mohd Mansor, H., Waheed Tajudeen, N. F. and Nordin, N. (2020) Adsorption kinetics for carbon dioxide capture using bismuth(III) oxide impregnated on activated carbon. *Malaysian J. Chem.*, **22**, 1, 33–46.

58. Araújo, J. C., Ferreira, D. P., Teixeira, P. and Fangueiro, R. (2021) In-situ synthesis of CaO and SiO_2 nanoparticles onto jute fabrics: exploring the multifunctionality. *Cellulose*, **28**, 2, 1123–1138, Jan. 2021.

59. Singh, V., Mandal, T., Mishra, S. R., Singh, A. and Khare, P. (2024) Development of amine-functionalized fluorescent silica nanoparticles from coal fly ash as a sustainable source for nanofertilizer *Sci. Rep.*, **14**, 1, 1–13, Feb. 2024.

60. Mikolaszek, B., Jamrógiewicz, M., Mojsiewicz-Pieńkowska, K. and Sznitowska, M. (2022) Microscopic and spectroscopic imaging and thermal analysis of acrylates, silicones and active pharmaceutical ingredients in adhesive transdermal patches. *Polymers (Basel)*, **14**, 14, 2888, Jul. 2022.

61. Ernawati, L., Wahyuono, R. A., Laksono, A. D., Ningrum, A., Handayani, K. and Sabrina, A. (2021) Wollastonite ($CaSiO_3$)-based composite particles for synthetic food dyes (brilliant blue) removal in aquatic media: Synthesis, characterization and kinetic study. *IOP Conf. Ser. Mater. Sci. Eng.*, **1053**, 1, 012001.

62. Mardina, D., Asmi, D., Badaruddin, M. and Syahrial, A. Z. (2021) Preparation of synthetic β-wollastonite produced from amorphous sio2 bamboo leaf ash and meretix meretix shell. In *Materials Science Forum*, *1029 MSF*, 167–173.

63. Shariatmadar Tehrani, F., Goh, B. T., Muhamad, M. R. and Rahman, S. A. (2013) Pressure dependent structural and optical properties of silicon carbide thin films deposited by hot wire chemical vapor deposition from pure silane and methane gases. *J. Mater. Sci. Mater. Electron.*, **24**, 4, 1361–1368, Apr. 2013.

64. Silva, F. A. B., Aparecida, F., Florenzano, F. and Pisetti, F. (2016) Poly(dimethylsiloxane) and Poly[vinyltrimethoxysilane-co-2-(dimethylamino) ethyl methacrylate] Based Cross-Linked Organic-Inorganic Hybrid Adsorbent for Copper(II) Removal from A. *Journal Brazilian Chem. Soc.*, 1–11, January, 2016.

65. Lahuri, A. H., Yarmo, M. A. and Tahari, M. N. A. (2021) Ultrasonic assisted synthesis of bimetal composite strontium oxide/iron(III) oxide for the adsorption isotherm analysis of CO_2 capture. *Lect. Notes Mech. Eng.*, 175–195.

66. Silva, F. A. B., Chagas-Silva, F. A., Florenzano, F. H. and Pissetti, F. L. (2016) Poly(dimethylsiloxane) and poly[vinyltrimethoxysilane-co-2-(dimethylamino) ethyl methacrylate] based cross-linked oroganic-inorganic hybrid adsorbent for copper(II) removal from aqueous solutions. *J. Braz. Chem. Soc.*, **27**, 12, 2181–2191, Jan. 2016.

67. Lahuri, A. H. and Yarmo, M. A. (2022) Study of CO_2 adsorption time for carbonate species and linear CO_2 formations onto bimetallic CaO/Fe_2O_3 by infrared spectroscopy. *Sains Malaysiana*, **51**, 2, 507–517.

68. Lahuri, A. H., Yarmo, M. A., Nordin, N., Dzakaria, N., Ing, A. H. I. and Kuda, S. J. S. (2023) Adsorption isotherm and surface analysis for the carbonate formation on nano coral-shaped iron(III) oxide. *Sains Malaysiana*, **52**, 1, 129–138, Jan. 2023.

69. Ganesapillai, M. and Simha, P. (2015) The rationale for alternative fertilization: Equilibrium isotherm, kinetics and mass transfer analysis for urea-nitrogen adsorption from cow urine. *Resour. Technol.*, **1**, 2, 90–97, Dec. 2015.

70. Arunkumar, C., Perumal, R., Lakshmi Naranayan, S. and Arunkumar, J. (2014) Use of corn cob as low cost adsorbent for the removal of nickel(II) from aqueous solution. *Int. J. Adv. Biotechnol. Res.*, **5**, 3, 325–330.

71. Pillai, M. G., Simha, P. and Gugalia, A. (2014) Recovering urea from human urine by bio-sorption onto microwave activated carbonized coconut shells: Equilibrium, kinetics, optimization and field studies. *J. Environ. Chem. Eng.*, **2**, 1, 46–55, Mar. 2014.

72. Köster, K., Wendt, H., Gallus, J., Krisam, G. and Lehmann, H. D. (1983) Regeneration of hemofiltrate by anodic oxidation of urea. *Artif. Organs*, **7**, 2, 163–168.

73. Simha, P., Ramanathan, A., Thawani, B., Jain, P., Hussain, S. and Ganesapillai, M. (2019) Coal fly ash for the recovery of nitrogenous compounds from wastewater: Parametric considerations and system design. *Arab. J. Chem.*, **12**, 8, 5049–5061.

74. Nguyen, C. H., Fu, C. C., Chen, Z. H., Van Tran, T. T., Liu, S. H. and Juang, R. S. (2021) Enhanced and selective adsorption of urea and creatinine on amine-functionalized mesoporous

silica SBA-15 via hydrogen bonding. *Microporous Mesoporous Mater.*, **311**, Feb. 2021.

75. Ruiz-Bastidas, R. C., Turnes, G., Palacio, E. and Cadavid-Rodríguez, L. S. (2023) Natural Ecuadorian zeolite: An effective ammonia adsorbent to enhance methane production from swine waste. *Chemosphere*, **336**, 139098, June, 2023.

76. Kumar, D., Rizal, U., Das, S., Swain, B. S. and Swain, B. P. (2018) Micro-raman and FTIR analysis of silicon carbo-nitride thin films at different H_2 flow rate. *Lect. Notes Electr. Eng.*, **443**, 77–83.

77. Cheah, W. K., Sim, Y. L. and Yeoh, F. Y. (2016) Amine-functionalized mesoporous silica for urea adsorption. *Mater. Chem. Phys.*, **175**, 151–157.

78. Stern, T. (2020) Side-reactions in diisocyanate-derived bulk polyurea synthesis. *J. Appl. Polym. Sci.*, **137**, 35, 1–16.

79. Jafari, S., Hirsch, J., Lausch, D., John, M., Bernhard, N. and Meyer, S. (2019) Composition limited hydrogen effusion rate of a-SiN x :H passivation stack. *AIP Conf. Proc.*, **2147**, 050004.

80. Lahuri, A. H., Yusuf, A. M., Adnan, R., Rahim, A. A., Waheed Tajudeen, N. F. and Nordin, N. (2022) Kinetics and thermodynamic modeling for CO_2 capture using NiO supported activated carbon by temperature swing adsorption. *Bio-interface Res. Appl. Chem.*, 12, 3, 4200–4219.

81. Zhu, N., Qian, F., Xu, X., Wang, M. and Teng, Q. (2021) Thermogravimetric experiment of urea at constant temperatures. *Mater.*, **14**, 20, 6190, Oct. 2021.

82. Azizul Hakim, L., Mohd. Ambar, Y., Maratun Najiha, A. T. and Norliza, D. (2022) Adsorption isotherm analysis for CO_2 capture using barium oxide impregnated iron(III) oxide by ultrasonic-assisted synthesis. *Key Eng. Mater.*, **908**, 379–384.

83. Jones, J. M. and Rollinson, A. N. (2013) Thermo-gravimetric evolved gas analysis of urea and urea solutions with nickel alumina catalyst. *Thermochim. Acta*, **565**, 39–45, Aug. 2013.

84. Razali, N., Jumadi, N., Jalani, A. Y., Kamarulzaman, N. Z. and Pa'ee, K. F. (2022) Thermal decomposition of calcium carbonate in chicken eggshells: Study on temperature and contact time. *Malaysian J. Anal. Sci.*, **26**, 2, 347–359.

85. Lahuri, A. H., Nguang Khai, M. L., Rahim, A. A. and Nordin, N. (2020) Adsorption kinetics for CO_2 capture using cerium oxide impregnated on activated carbon. *Acta Chim. Slov.*, **67**, 2, 570–580.